Synthesis and Characterization of Alkylammonium Hyponitrites and Base-Stabilized Hyponitrous Acid Salts

Navamoney Arulsamy, D. Scott Bohle,* Jerome A. Imonigie, and Elizabeth S. Sagan

Department of Chemistry, University of Wyoming, Laramie, Wyoming 82071-3838

Received November 20, 1998

A number of alkylammonium and bipyridinium salts of hyponitrous acid, namely, *N*,*N*,*N*′,*N*′-tetraethylethylenediammonium (**3** and **4**), *N*,*N*,*N*′,*N*′-tetramethylethylenediammonium (**5**), triethylenediammonium (**6**), diquinuclidinium (**7**), 2,2′-bipyridinium (**8**), 4,4′-bipyridinium (**9**), 4,4′-trimethylenebis(1-methylpiperidinium) (**10**), 4,4′-trimethylenepiperidinium (**11**), and bis(triethylammonium) (**12**) hyponitrite salts, have been synthesized by the reaction of the corresponding amine in either anhydrous diethyl ether or absolute ethanol with hyponitrous acid solution in anhydrous diethyl ether. Single-crystal X-ray crystallographic data were obtained for sodium hyponitrite (**1**), and the thermal decomposition behavior of the salt was examined. The new salts were characterized by IR and Raman spectroscopic data and elemental analyses. Compounds **4** and **7**−**9** were also characterized by single-crystal X-ray crystallography. The hyponitrite anions in **1** and **7**−**9** exhibit similar structural features. The anions are planar with average N═N and N−O bond distances of 1.237 and 1.380 Å, respectively. The monoprotonated hyponitrite anion and solvated hyponitrous acid molecules present in **4** also exhibit close structural similarity to the dianion in the crystals of **1** and **7**−**9**. Most of these salts are soluble in organic solvents. The UV−vis spectra of the sodium and alkylammonium salts (**1**, **3**−**7**, and **10**−**12**) in aqueous 0.1 M NaOH exhibit an absorption peak at 248 nm (λ_{max}) with a molar extinction coefficient of 7033 ± 153 M^{-1} cm^{-1}. Differential scanning calorimetric data for the salts reveal exothermic decomposition of the hyponitrite species. Significantly, the pentahydrate and anhydrous forms of $Na_2N_2O_2$ exhibit distinct thermal decomposition behavior. The thermogram of the pentahydrate exhibits two exotherms at ca. 96 and 382 °C, whereas that of the anhydrous $Na_2N_2O_2$ exhibits a single exotherm at ca. 382 °C. The exotherm at 96 °C observed for the pentahydrate is explained in terms of a coupled phase transition−dehydration process. The alkylammonium and bipyridinium salts undergo exothermic decomposition at a considerably lower temperature in the range 67−170 °C. Electrochemistry of the salts in acetonitrile solvent reveal an irreversible oxidation at ∼1.80 V vs an Ag/AgCl reference electrode.

Introduction

There is a substantial body of evidence which supports the hypothesis that peroxynitrite, $ONOO^-$, is formed from NO and O_2^- released by cytokine-activated macrophages.[1] Thus, this unusual peroxide is a critical component of the cell-killing cytotoxic flux from these cells. Chemical and physical characterization of this cytotoxin in vitro has been very elusive owing to its high reactivity and its short lifetime at physiological pH. Recently, we reported a solid-state synthesis of peroxynitrite with high purity,[2] but the structural characterization of this salt has been limited to vibrational and NMR spectral data correlated with theory. The hyponitrite dianion, $[ONNO]^{2-}$, is isoelectronic with peroxynitrite and is considerably less reactive. Hyponitrite and peroxynitrite anions can exist in either trans or cis configurations as shown in Figure 1. However, *trans*-hyponitrite is known to be more kinetically stable and is the only isolated conformer in the most widely used preparative method,[3] NO_2^- reduction with Na/Hg. Despite the wealth of information on the chemistry of hyponitrite species, the crystal structure of a simple *trans*-hyponitrite salt is unknown. Although the structure of *cis*-sodium hyponitrite was recently reported from X-ray

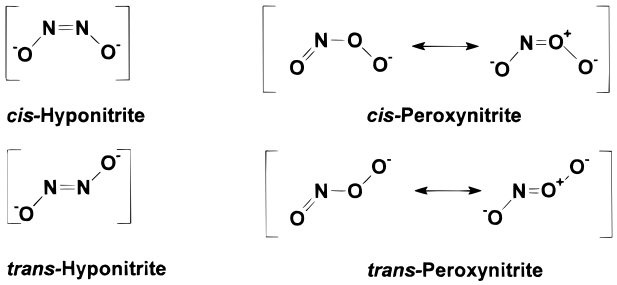

Figure 1. Electronic relationships in the four-atom oxyanions of nitrogen.

(1) (a) Beckman, J. S. *Nature* **1990**, *345*, 27. (b) Beckman, J. S.; Beckman, T. W.; Chen, J.; Marshall, P. A.; Freeman, B. A. *Proc. Natl. Acad. Sci. U.S.A.* **1990**, *87*, 1620. (c) Hogg, N.; Darley-Usmar, V. M.; Wilson, M. T.; Moncada, S. *Biochem. J.* **1992**, *28*, 419. (d) Ischiropoulos, H.; Zhu, L.; Beckman, J. S. *Arch. Biochem. Biophys.* **1992**, *298*, 446. (e) Radi, R.; Beckman, J. S.; Bush, K.; Freeman, B. A. *J. Biol. Chem.* **1991**, *266*, 4244. (f) Radi, R.; Cosgrove, T. P.; Beckman, J. S.; Freeman, B. A. *J. Biol. Chem.* **1993**, *290*, 51. (g) Beckman, J. S.; Ye, Y. Z.; Anderson, P. G.; Chen, J.; Accavitti, M. A.; Tarpey, M. M.; White, C. R. *Biol. Chem. Hoppe-Seyler* **1994**, *375*, 81. (h) Wang, P.; Zweier, J. L. *J. Biol. Chem.* **1996**, *271*, 29223.

(2) Bohle, D. S.; Hansert, B.; Paulson, S. C.; Smith, B. D. *J. Am. Chem. Soc.* **1994**, *116*, 7423.

(3) (a) Hughes, M. N. *Q. Rev., Chem. Soc.* **1968**, *22*, 1. (b) McGraw, G. E.; Bernitt, D. L.; Hisatsune, I. C. *Spectrochim. Acta A* **1967**, *23*, 25.

(4) (a) Feldmann, C.; Jansen, M. *Angew. Chem., Int. Ed. Engl.* **1996**, *35*, 1728. (b) Feldmann, C.; Jansen, M. *Z. Allg. Anorg. Chem.* **1997**, *623*, 1803.

(5) (a) Millen, D. J.; Polydoropoulos, C. N.; Watson, D. *J. Chem. Soc.* **1960**, 687. (b) Kuhn, L.; Lippincott, E. R. *J. Am. Chem. Soc.* **1956**, *78*, 1820. (c) Rauch, J. E.; Decius, J. C. *Spectrochim. Acta*, **1966**, *22*, 1963. (d) Hughes, M. N. *J. Inorg. Nucl. Chem.* **1967**, *29*, 1376.

10.1021/ic981340c CCC: $18.00
Published on Web 05/14/1999

powder diffraction studies,[4] the structure suggested for *trans*-sodium hyponitrite is based on vibrational spectroscopic evidence.[3,5] However, several complexes with bridging *trans*-[6] and *cis*-hyponitrite[7] ligands have been crystallographically characterized. Given the renewed interest in this class of compounds, we sought to establish their characterization more firmly.

One of the most plausible reasons for the absence of crystal structures of simple *trans*-hyponitrite salts is their preparative methods which often result in contamination with carbonates.[8] As a result of these gross impurities associated with sodium hyponitrite, there have been many discrepancies in the reported molar extinction coefficients[8,9] as well as the thermal behavior of its salts.[3a,4,9a,10] In addition, there are no known simple hyponitrite anions that are stable at room temperature and soluble in organic solvents. In this paper, we report (1) the first crystal structural determination of *trans*-sodium hyponitrite, (2) the first thermal decomposition behavior of crystalline *trans*-sodium hyponitrite and characterization of several of its phases, (3) the synthesis, the characterization, and the first crystal structures of novel alkylammonium hyponitrites and base-stabilized hyponitrous acid salts which are stable at room temperature and soluble in a variety of organic solvents, (4) the DSC, UV−vis, IR, and Raman spectroscopic results for these ions, and (6) the first electrochemical studies of the hyponitrite anion.

Experimental Section

Materials and Methods. All chemicals and solvents were of reagent grade and were used without further purification except triethylamine, which was purified by stirring in KOH overnight under nitrogen atmosphere and distilled from calcium hydride. For inert-atmosphere operations, solvents were dried, distilled, and degassed by standard techniques.[11] IR spectra were recorded on an MIDAC FTIR instrument as potassium bromide pellets. Raman spectra were recorded on a Detection Limit, Inc., Solution 633 Raman laser system. UV−vis data were measured at room temperature on a Hewlett-Packard 8452 diode-array spectrometer with quartz cuvettes. ^{1}H and ^{13}C NMR spectra were recorded at 400 MHz at room temperature using either $CDCl_3$ or $(CD_3)_2SO$ with 0.05% (v/v) TMS as internal reference. Elemental analyses were performed by Atlantic Microlab, Norcross, GA. All the reported yields for the base-stabilized hyponitrites are estimated from the amount of $Ag_2N_2O_2$ used to neutralize hydrochloric acid in the reaction mixture. Since $Ag_2N_2O_2$ was used in excess to ensure complete neutralization of the hydrochloric acid, the exact amount of $Ag_2N_2O_2$ consumed in the reactions is only a rough estimate.

Synthesis of $Na_2N_2O_2 \cdot 5H_2O$ (1). Sodium hyponitrite was prepared according to a modified literature method by the reduction of sodium nitrite with sodium amalgam,[12] which was prepared according to a literature method.[13] The reaction mixture containing sodium hyponitrite was transferred into a three-necked round-bottom flask containing ice-chilled ethanol, and a steady stream of nitrogen gas was passed through the headspace with constant stirring. After being stirred for ca. 30 min, the solution was further cooled in an ice bath for ca. 2 h. The white crystalline sodium hyponitrite formed was filtered off, washed successively with absolute ethanol and diethyl ether, and dried in a desiccator over P_2O_5 or in vacuo over P_2O_5. Sodium hyponitrite crystals suitable for X-ray analysis were obtained as above except that the sodium hyponitrite solution was cooled at −28 °C for 1 d.

Synthesis of $Ag_2N_2O_2$ (2). Silver hyponitrite was prepared by the slow addition of an aqueous solution of a substoichiometric amount of $AgNO_3$ to an aqueous solution of sodium hyponitrite with constant stirring. If exact stoichiometric quantities of sodium hyponitrite pentahydrate and silver nitrate are used, the resulting silver hyponitrite is contaminated with elemental silver and takes on a greenish sheen. As an example of a preparation of pure silver hyponitrite, 0.8498 g, 0.0043 mol, of $Na_2N_2O_2 \cdot 5H_2O$ was dissolved in 50 mL of water and the solution was cooled on ice. A solution of 0.9029 g, 0.0053 mol, of $AgNO_3$ in 20 mL water was then added dropwise, and the bright yellow suspension was stirred for 20 min. The bright canary-yellow precipitate, 0.731 g, 65% yield, was filtered off, thoroughly washed with anhydrous ethanol and anhydrous diethyl ether, and dried in vacuo over P_2O_5.

Synthesis of the $H_2N_2O_2$ Solution. To 20 mL of anhydrous diethyl ether solution saturated with dry hydrogen chloride gas was slowly added, with stirring, dry $Ag_2N_2O_2$ (3.42 g, 10.89 mmol) at ice-bath temperature until the canary-yellow solid $Ag_2N_2O_2$ persisted.[14,15] The precipitated AgCl was removed by filtration, and the filtrate containing hyponitrous acid was further chilled in an ice bath before addition of base (see below). ***Caution!*** *Solid hyponitrous acid is potentially explosive.*[3a,14] *Isolation of hyponitrous acid in more than 50 mg quantities could be dangerous.*

Synthesis of $[HEt_2NCH_2CH_2NEt_2H][N_2O_2]$ (3). To 20 mL of an ice-chilled anhydrous diethyl ether solution of hyponitrous acid (1.03 g, 16.7 mmol) was added dropwise an excess of *N*,*N*,*N*′,*N*′-tetraethylethylenediamine solution (3.45 g, 20 mmol) in 10 mL of anhydrous diethyl ether with stirring. An immediate white crystalline precipitate was formed. The solid redissolved in the solvent when the mixture was warmed to room temperature. The solution was stirred for ca. 30 min and cooled at −56 °C for 24 h, whereupon a white crystalline precipitate was formed. The precipitate was filtered off and dried in vacuo over P_2O_5. More crystalline solid was obtained on cooling the filtrate at −56 °C for several days. *Note: If the N,N,N′,N′-tetraethylethylenediamine solution is added rapidly, the yield is greatly reduced* (yield: 1.79 g, 46%). Anal. Calcd for $C_{10}H_{26}N_4O_2$: C, 51.28; H, 11.11; N, 23.93. Found: C, 51.30; H, 11.05; N, 23.98. IR (KBr): 3437 b, 2984 s, 2938 m, 2861 m, 2702 b, 2591 b, 1819 b, 1566.3 m, 1467.9 vs, 1448.6 vs, 1388.8 m, 1375.3 s, 1350.3 w, 1327 w, 1294 w, 1267 m, 1196 m, 1146 m, 1117 s, 1080 m, 1055 s, 1042 s, 1000 vs, 976 vs, 905 w, 878 w, 824 m, 793 m, 741 vs, 577 vs, 480 sh, 463 s, 438 sh cm^{-1}. Raman: 1449 vs, 1388 m, 1307 m, 1191 vw, 1140 vw, 1071 m, 1054 m, 1020 s, 990 w, 895 s, 823 w, 779 s, 639 vs, 547 vw, 522 w, 380 w, 264 m cm^{-1}. UV−vis (0.1 M NaOH solution; λ_{max}, nm (ϵ)): 248 (7256 ±150 M^{-1} cm^{-1}). ^{1}H NMR ($(CD_3)_2SO$): δ 0.93 (t, 3H, J = 7.08 Hz), 2.44 (q, 2H, J = 7.12 Hz), 2.41 (s, 4H), 12.4 (s, b, 2H). ^{13}C NMR ($(CD_3)_2SO$): δ 11.9, 46.9, 50.7.

Synthesis of $[HEt_2NCH_2CH_2NEt_2H][HN_2O_2]_2 \cdot H_2N_2O_2$ (4). This compound was prepared by the same procedure described for the synthesis of **3** by dropwise addition of less than the stoichiometric amount of *N*,*N*,*N*′,*N*′-tetraethylethylenediamine solution (0.839 g, 4.87 mmol) to a solution of hyponitrous acid (0.380 g, 6.14 mmol). Crystals suitable for X-ray analysis were prepared by dissolving the resulting precipitate in a 2:1 diethyl ether/hexane solution and cooling at −28 °C for 2 d (yield: 792 mg, 36%). The crystals underwent slow decomposition at room temperature. Consequently, the crystals dried in vacuo at room temperature analyzed for the formula $[HEt_2NCH_2CH_2NEt_2H][HN_2O_2]_2$, indicating the loss of the $H_2N_2O_2$ solvate. Anal.

(6) Bau, R.; Sabherwal, I. H.; Burg, A. B. *J. Am. Chem. Soc*. **1971**, *93*, 4926.
(7) (a) Hoskins, B. F.; Whillans, F. D.; Dale, D. H.; Hodgkin, D. C. *Chem. Commun*. **1969**, 69. (b) Bhaduri, S.; Johnson, B. F. G.; Pickard, A.; Raithby, P. R.; Sheldrick, G. M.; Zuccaro, C. I. *J. Chem. Soc., Chem. Commun*. **1977**, 354.
(8) Bonner, F. T.; Hughes, M. N. *Comments Inorg. Chem*. **1988**, *7*, 215.
(9) (a) Addison, C. C.; Gamlen, G. A.; Thompson, R. *J. Chem. Soc*. **1952**, 338. (b) Polydoropoulos, C. N.; Voliotis, S. D. *Anal. Chim. Acta* **1968**, *40*, 170. (c) Conner, C. N.; Donald, C. E.; Hughes, M. N.; Sami, C. *Polyhedron* **1989**, *8*, 2621.
(10) (a) Goubeau, V. J.; Laitenberger, K. *Z. Anorg. Allg. Chem*. **1963**, *320*, 78. (b) Picugina, N. G.; Aleshin, V. V.; Shirokova, G. N.; Rosolovskii, V. Y. *Russ. J. Inorg. Chem*. **1985**, *30*, 494. (c) Abata, J. D.; Dziobak, M. P.; Nachbor, M.; Mendenhall, G. D. *J. Phys. Chem*. **1989**, *93*, 3368 and references therein.
(11) Perrin, D. D.; Armarego, W. L. F. *Purification of Laboratory Chemicals*, 3rd ed.; Pergamon Press: Oxford, U.K., 1988.
(12) Addison, C. C.; Gamlen G. A.; Thompson, R. *J. Chem. Soc*. **1952**, 338.
(13) Neuman, R. C., Jr.; Bussey, R. J. *J. Am. Chem. Soc*. **1970**, *92*, 2440.
(14) Brauer, G. *Handbook of Preparative Inorganic Chemistry*; Academic Press: New York, 1963; Vol. 1, p 493.
(15) Pichugina, N. G.; Aleshin, V. V.; Rosolovskii, V. Ya. *Russ. J. Inorg. Chem*. **1985**, *30*, 494.

Calcd for $C_{10}H_{28}N_6O_4$: C, 40.54; H, 9.46; N, 28.38. Found: C, 40.25; H, 9.25; N, 28.57. IR (KBr): 3177 b, 2985 m, 2805 w, 2708 w, 2594 b, 2239 m, 1805 b, 1545 m, 1502 m, 1471 m, 1452 m, 1399 m, 1388 m, 1376 m, 1324 vw, 1304 vw, 1268 vw, 1173 w, 1076 s, 1010 vs, 988 vs, 962 vs, 834 s, 807 m, 742 w, 668 m, 657 s, 578 w, 521 w, 465 s cm^{-1}. UV−vis (0.1 M NaOH solution; λ_{max}, nm (ϵ)): 248 (7100 ± 60 M^{-1} cm^{-1}).

Synthesis of $[HMe_2NCH_2CH_2NMe_2H][N_2O_2]$ (5). This compound was prepared as described for compound **3** by dropwise addition of an excess of *N*,*N*,*N*′,*N*′-tetramethylethylenediamine solution (1.8 g, 15.5 mmol) to a solution of hyponitrous acid (0.674 g, 10.87 mmol). An immediate white precipitate was formed (yield: 910 mg, 47%). Anal. Calcd for $C_6H_{18}N_4O_2$: C, 40.40; H, 10.10; N, 31.42. Found: C, 40.73; H, 10.11; N, 31.42. IR (KBr): 3207 m, b, 2997 w, 2960 w, 1557 b, 1464 w, 1425 w, 1353 w, 1279 m, 1261 m, 1165 m, 1145 m, 1099 m, 1020 vs, 1037 vs, 989 vs, 831 vs, 789 vs, 504 vs, 463 vs cm^{-1}. UV−vis (0.1 M NaOH solution; λ_{max}, nm (ϵ)): 248 (6960 ± 50 M^{-1} cm^{-1}). ^1H NMR ($(CD_3)_2SO$): δ 2.21 (s, 12H), 2.28 (s, 4H), 12.4 (s, b, 2H). ^{13}C NMR ($(CD_3)_2SO$): δ 45.5, 57.1.

Synthesis of $[(CH_2CH_2)_3N_2H_2][N_2O_2]$ (6). This compound was prepared as described for compound **3** by dropwise addition of an excess of 1,4-diazabicyclo[2.2.2]octane (DABCO) solution (1.8 g, 16 mmol) to a solution of hyponitrous acid (0.561 g, 9.06 mmol). An immediate white precipitate insoluble in diethyl ether solution was formed. The product was recrystallized from warm absolute ethanol as colorless cubic crystals (yield: 951 mg, 60.32%). Anal. Calcd for $C_6H_{14}N_4O_2$: C, 41.37; H, 8.04; N, 32.16. Found: C, 40.63; H, 7.96; N, 31.62. IR (KBr): 3434 b, 2976 w, 2953 m, 2885 w, 2451 m, b, 1890 b, 1721 b, 1566 b, 1503 b, 1463 m, 1346 m, 1324 m, 1261 w, 1059 m, 1016 m, 999 vs, 835 sh, 745 sh, 778 vs, 461 vs cm^{-1}. Raman: 1452 m, 1394 w, 1296 w, 1079 w, 1056 w, 984 s, 800 vs, 669 w, 623 s, 573 w, 420 w, 270 m cm^{-1}. UV−vis (0.1 M NaOH solution; λ_{max}, nm (ϵ)): 248 (6820 ± 86 M^{-1} cm^{-1}).

Synthesis of [Quinuclidinium]$_2$$[N_2O_2]$ (7). This compound was prepared as described for compound **3** by dropwise addition of an excess of quinuclidine solution (4.0 g, 36 mmol) to a solution of hyponitrous acid (0.918 g, 14.8 mmol). An immediate white precipitate was formed. Suitable crystals for X-ray analysis were obtained by slow evaporation of the mother liquor at room temperature (yield: 1.92 g, 46%). Anal. Calcd for $C_{14}H_{28}N_4O_2$: C, 59.07; H, 9.86; N, 19.69. Found: C, 59.07; H, 10.03; N, 19.28. IR (KBr): 3443 b, 2948 w, 2922 w, 2873 w, 2237 w, 2216 w, 1896 b, 1825 w, 14733 sh, 1457 m, 1353 m, 1320 m, 1206 w, 1080 m, 1053 m, 1010 vs, 982 vs, 956 sh, 883 w, 830 m, 802 sh, 777 vs, 631 vs, 613 w, 465 vs cm^{-1}. Raman: 1453 m, 1371 w, 1274 w, 1199 w, 1118 m, 1077 m, 1042 s, 1028 s, 965 m, 889 m, 793 vs, 663 m, 638 m, 609 m, 534 w, 393 w, 270 m cm^{-1}. UV−vis (0.1 M NaOH solution; λ_{max}, nm (ϵ)): 248 (6950 ± 100 M^{-1} cm^{-1}). ^1H NMR ($CDCl_3$): δ 1.50−1.57 (m, 6H), 1.76 (sept, 1H, J = 3.17 Hz), 2.87 (t, 6H, J = 8.00 Hz), 6.53 (s, b, 2H). ^{13}C NMR ($CDCl_3$): δ 19.2, 22.9, 53.0.

Synthesis of [2,2′-Bipyridinium]$[N_2O_2]$ (8). This compound was prepared as described for compound **3** by dropwise addition of an excess of 2,2′-bipyridine solution (3.15 g, 20 mmol) to a solution of hyponitrous acid (0.719 g, 11.6 mmol). After ca. 5 min of stirring, a white precipitate insoluble in diethyl ether solution began to form. The mother liquor was allowed to evaporate slowly at room temperature, and large colorless needlelike crystals suitable for X-ray analysis were obtained (yield: 1.23 g, 49%). Anal. Calcd for $C_{10}H_{10}N_4O_2$: C, 54.99; H, 4.58; N, 25.67. Found: C, 54.99; H, 4.62; N, 25.54. IR (KBr): 3436 b, 3214 w, 3034 b, 2767 b, 2616 b, 1589 s, 1542 m, 1465 s, 1413 m, 1255 m, 1221 w, 1154 m, 1096 s, 1080 s, 1040 m, 1014 vs, 1004 vs, 989 vs, 916 w, 829 m, 765 vs, 634 vs, 546 vw, 460 vs cm^{-1}. ^1H NMR ($(CD_3)_2SO$): δ 7.45 (dd, 2H, J = 1.66, 3.69 Hz), 7.94 (dd, 2H, J = 1.69, 6.00 Hz), 8.38 (d, 2H, J = 8.00 Hz), 8.68 (d, 2H, J = 3.46 Hz), 12.4 (s, 2H). ^{13}C NMR ($(CD_3)_2SO$): δ 120, 124, 137, 149, 155.

Synthesis of [4,4′-Bipyridinium]$[N_2O_2]$ (9). This compound was prepared as described for compound **3** by dropwise addition of an excess of 4,4′-bipyridine solution (4.4 g, 28.2 mmol) in absolute ethanol to a solution of hyponitrous acid (0.806 g, 13 mmol). An immediate white precipitate insoluble in diethyl ether solution was formed (yield: 1.36 g, 48%). Suitable crystals for X-ray analysis were obtained by dissolving the white precipitate in 4 mL of an anhydrous ethanol/acetonitrile (1:1) mixture, followed by slow addition of diethyl ether to initiate recrystallization. Anal. Calcd for $C_{10}H_{10}N_4O_2$: C, 54.99; H, 4.58; N, 25.67. Found: C, 55.05; H, 4.63; N, 25.62. IR (KBr): 3453 b, 3192 b, 2998 b, 2698 b, 2577 b, 1751 w, 1601 m, 1559 m, 1412 m, 1321 w, 1219 m, 1069 m, 986 vs, 905 s, 854 w, 809 vs, 623 vs, 572 vs, 509 s, 456 vs cm^{-1}. ^1H NMR ($(CD_3)_2SO$): δ 7.83 (d, 2H, J = 2.98 Hz), 8.72 (d, 2H, J = 2.99 Hz), 12.4 (s, 2H). ^{13}C NMR ($(CD_3)_2SO$): δ 121, 144, 150.

Synthesis of [4,4′-Trimethylenebis(1-methylpiperidinium)]$[N_2O_2]$ (10). This compound was prepared as described for compound **3** by dropwise addition of an excess of 4,4′-trimethylenebis(1-methylpiperidine) solution (3.5 g, 14.7 mmol) to a solution of hyponitrous acid (0.534 g, 8.62 mmol). An immediate white precipitate insoluble in diethyl ether solution was formed (yield: 1.61 g, 61%). Anal. Calcd for $C_{15}H_{32}N_4O_2$: C, 59.92; H, 10.65; N, 18.64. Found: C, 60.12; H, 10.70; N, 18.63. IR (KBr): 3437 b, 2934 m, 2854 m, 2801 m, 2583 b, 1825 b, 1551 b, 1459 m, 1447 m, 1419 w, 1381 m, 1280 s, 1274 s, 1255 sh, 1190 w, 1165 m, 1142 s, 1110 m, 1100 m, 1076 m, 1043 sh, 1001 vs, 973 m, 963 m, 919 vw, 877 w, 830 m, 802 w, 767 vs, 730 w, 602 w, 460 vs, 412 m cm^{-1}. UV−vis (0.1 M NaOH solution; λ_{max}, nm (ϵ)): 248 (7146 ± 45 M^{-1} cm^{-1}).

Synthesis of [4,4′-Trimethylenedipiperidinium]$[N_2O_2]$ (11). This compound was prepared as described for compound **3** by dropwise addition of an excess of 4,4′-trimethylenepiperidine solution (4.8 g, 22.8 mmol) in absolute ethanol to a solution of hyponitrous acid (0.837 g, 13.5 mmol). An immediate white precipitate insoluble in diethyl ether solution was formed (yield: 1.65 g, 45%). Anal. Calcd for $C_{13}H_{28}N_4O_2$: C, 57.28; H, 10.28, N, 20.56. Found: C, 57.38; H, 10.36; N, 20.55. IR (KBr): 3442 b, 3288 m, 3272 m, 2939 m, 2853 m, 2483 b, 1620 b, 1457 w, 1444 w, 1318 w, 1274 w, 1237 sh, 1162 w, 1110 w, 1010 vs, 970 sh, 900 w, 850 vs, 799 m, 726 vw, 624 vw, 518 w, 459 vs cm^{-1}. UV−vis (0.1 M NaOH solution; λ_{max}, nm (ϵ)): 248 (6882 ± 120 M^{-1} cm^{-1}).

Synthesis of $[Et_3NH]_2[N_2O_2]$ (12). This compound was prepared as described for compound **3** by dropwise addition of an excess of anhydrous triethylamine solution in anhydrous diethyl ether (1.8 g, 27.8 mmol) to a solution of hyponitrous acid (0.062 g, 10 mmol). The solvent was removed in vacuo. The product obtained as a white residue was thermally unstable at room temperature. Therefore, a satisfactory elemental analysis could not be obtained for this compound. IR and UV−vis spectral data measured within 3 h were, however, consistent with the structure (yield: 1.48 g, 56%). IR (KBr): 1546 s,1509 s, 1468 s, 1407 m, 1387 m, 1268 m, 1179 m, 1089 s, 1045 sh, 979 vs, 845 s, 804 s, 670 s, 613 w, 560 w, 462 s cm^{-1}. Raman: 1471 w, 1409 vs, 1294 w, 1255 m, 1151 m, 1025 s, 874 w, 737 m, 67 w, 623 w, 419 m, 409 m, 296 m cm^{-1}. UV−vis (0.1 M NaOH solution; λ_{max}, nm (ϵ)): 248 (7160 ± 50 M^{-1} cm^{-1}). ***Caution!*** *If triethylamine is not added in excess, a mixture of hyponitrous acid and monoprotonated hyponitrite is produced which decomposes violently on exposure to air.*

Thermal Analysis. Thermal analysis measurements were carried out in a TA Instruments DSC 2010 differential scanning calorimeter equipped with a liquid nitrogen cooling accessory. About 2−5 mg of sample was loaded into an aluminum sample cup for each run. The thermal cycle was performed using a 10 °C/min heating rate under an argon atmosphere from −100 to +500 °C. The temperature and heat content were calibrated using the melting transition of indium (T_m = 156.6 °C). The heat exchanger installed on the DSC cell allows for the measurements of the thermal properties during heating and cooling.

Electrochemistry. All cyclic and square-wave voltammetric experiments were performed with a BAS-50W potentiostat in an inert-atmosphere box. In each case, the cell consisted of a platinum-button working electrode, a platinum-wire auxiliary electrode, and an Ag/$AgNO_3$/CH_3CN reference electrode with 0.1 M tetra-*n*-butylammonium

Table 1. Crystallographic Data for **1**, **4**, and **7**−**9**

	1	**4**	**7**	**8**	**9**
empirical formula	$Na_2N_2O_2{\cdot}5H_2O$	$C_{10}H_{30}N_8O_6$	$C_{14}H_{28}N_4O_2$	$C_{10}H_{10}N_4O_2$	$C_{10}H_{10}N_4O_2$
fw	214.10	358.42	284.40	218.22	218.22
λ, Å	0.710 73	0.710 73	0.710 73	0.710 73	0.710 73
space group	$P2_1/c$	$C2/c$	$P2_1/c$	$C2/c$	$P2_1/c$
a, Å	6.1022(6)	12.9607(11)	10.658(2)	15.7370(10)	12.996(2)
b, Å	5.9499(8)	7.1936(6)	6.4440(10)	3.765	14.218(2)
c, Å	11.565(2)	20.868(3)	11.685(2)	18.640(2)	11.856(2)
α, deg	90	90	90	90	90
β, deg	92.508(10)	105.826(7)	93.730(10)	113.590(10)	111.314(11)
γ, deg	90	90	90	90	90
V, Å^3	419.49(10)	1871.9(3)	800.8(2)	1012.12(13)	2040.9(5)
Z	2	4	2	4	8
μ, mm^{-1}	0.257	0.104	0.080	0.105	0.104
ρ_{calcd}, g cm^{-3}	1.695	1.272	1.179	1.432	1.420
T, °C	−100	−100	−100	−100	−100
S_{gof}	1.088	1.039	1.074	1.109	1.047
$R1^a$ [$F > 2\sigma F$]	0.0190	0.0552	0.0534	0.0302	0.0565
w$R2^b$	0.0516	0.1480	0.1442	0.0807	0.1124

Table 2. Selected Bond Lengths and Angles for **1**, **4**, and **7**−**9**, the Ionic Bond of **1**, and the Hydrogen Bonds of **4** and **7**−**9**

compd	fragment	N═N, Å		N−O, Å		N−N−O, deg		other parameters, Å (ionic and H-bonds)	
1	$[ONNO]^{2-}$	N(1)−N(1)	1.256(2)	N(1)−O(1)	1.3622(11)	N(1)−N(1)−O(1)	112.14(9)	Na(1)···O(1)	2.5178(8)
4	$[HONNO]^-$	N(1)−N(2)	1.232(3)	N(1)−O(1)	1.371(3)	N(2)−N(1)−O(1)	110.1(2)	N(4)···O(1)	2.726(3)
				N(2)−O(2)	1.402(3)	N(1)−N(2)−O(2)	108.2(2)	O(1)···O(2)	2.648(3)
	HONNOH	N(3)−N(3)	1.226(4)	N(3)−O(3)	1.363(3)	N(3)−N(3)−O(3)	109.9(3)	O(1)···O(3)	2.592(3)
7	$[ONNO]^{2-}$	N(1)−N(1)	1.224(4)	N(1)−O(1)	1.358(3)	N(1)−N(1)−O(1)	110.5(2)	N(2)···O(1)	2.624(3)
8	$[ONNO]^{2-}$	N(1)−N(1)	1.233(2)	N(1)−O(1)	1.3887(13)	N(1)−N(1)−O(1)	107.64(11)	N(2)···O(1)	2.7343(13)
9	$[ONNO]^{2-}$	N(1)−N(2)	1.236(4)	N(3)−O(3)	1.393(4)	N(2)−N(1)−O(1)	109.0(3)	N(8)···O(3)	2.706(4)
				N(4)−O(4)	1.390(4)	N(1)−N(2)−O(2)	107.6(3)	N(6)···O(1)	2.697(4)
		N(3)−N(4)	1.238(4)	N(1)−O(1)	1.385(4)	N(4)−N(3)−O(3)	107.8(3)		
				N(2)−O(2)	1.387(4)	N(4)−N(4)−O(4)	108.1(3)		

hexafluorophosphate as the supporting electrolyte in acetonitrile. All reported potential values are referenced to the internal ferrocene/ferrocenium couple.

Ab Initio Calculations. The calculations described here were performed using Gaussian 98 implemented on a Silicon Graphics Iris Indigo workstation. Full optimizations were performed initially at the restricted Hartree−Fock (HF) level using the polarized split-valence 6-31G* basis sets before the final optimizations which were performed by density functional theory using Becke's three-parameter functional and triple split-valence basis sets, 6-311+G*.

Crystallographic Structure Determinations. X-ray diffraction data were collected for single crystals of $[Na_2N_2O_2{\cdot}5H_2O]$ (**1**), $[HEt_2NCH_2CH_2NEt_2H][HN_2O_2]_2{\cdot}H_2N_2O_2$ (**4**), [quinuclidinium][N_2O_2] (**7**), [2,2′-bipyridinium][N_2O_2] (**8**), and [4,4′-bipyridinium][N_2O_2] (**9**) on a Siemens P4 diffractometer equipped with a molybdenum tube [$\lambda(K\alpha_1)$ = 0.709 26 Å; $\lambda(K\alpha_2)$ = 0.713 54 Å] and a graphite monochromator at −100 °C. The crystals were mounted on a glass fiber using epoxy adhesive resin and were coated with Paratone N oil. The intensities of three standard reflections monitored every 100 reflections during the respective data collections indicated negligible crystal decomposition. The structures were solved by direct methods and refined by full-matrix least-squares techniques on F^2 using structure solution programs from the SHELXTL system.[16] Important crystallographic parameters are collected in Table 1. Selected interatomic distances and bond angles for **1**, **4**, and **7**−**9** are presented Table 2.

[$Na_2N_2O_2{\cdot}5H_2O$] (1). Data were collected for a colorless crystal of dimensions 0.22 × 0.40 × 0.81 mm. The compound crystallizes in the monoclinic space group $P2_1/c$ with 2 $Na_2N_2O_2{\cdot}5H_2O$ in the unit cell. A total of 732 (R_{int} = 0.0135) observed independent reflections [$F > 4\sigma(F)$] were collected in the 2θ range 6.68−50°, with the data gathered having $-1 \le h \le 7$, $7 \le k \le 1$, and $-13 \le l \le 13$. The data were not corrected for absorption. All hydrogen atoms were located in successive Fourier maps and refined isotropically, whereas the non-hydrogen atoms were refined anisotropically. The structure was refined by using the weighted least-squares process $w^{-1} = \sigma^2(F_o^2) + 0.0262^2 + 0.08P$, where $P = (F_o^2 + 4F_c^2)/3$. The maximum and minimum residual intensities remaining were 0.184 and −0.136 e Å^{-3}, respectively.

[$HEt_2NCH_2CH_2NEt_2H][HN_2O_2]_2{\cdot}H_2N_2O_2$ (4). Data were collected for a colorless crystal of dimensions 0.22 × 0.28 × 0.44 mm. The compound crystallizes in the monoclinic space group $C2/c$ with 4 [$HEt_2NCH_2CH_2NEt_2H][HN_2O_2]_2{\cdot}H_2N_2O_2$ in the unit cell. A total of 1640 (R_{int} = 0.0183) observed independent reflections [$F > 4\sigma(F)$] were collected in the 2θ range 4.06−50°, with the data gathered having $-1 \le h \le 15$, $-8 \le k \le 1$, and $-24 \le l \le 24$. The data were not corrected for absorption. All hydrogen atoms were located in successive Fourier maps and refined isotropically, whereas the non-hydrogen atoms were refined anisotropically. The structure was refined by using the weighted least-squares process $w^{-1} = \sigma^2(F_o^2) + 0.0763^2 + 4.54P$, where $P = (F_o^2 + 4F_c^2)/3$. The maximum and minimum residual intensities remaining were 0.777 and −0.211 e Å^{-3}, respectively.

[Quinuclidinium]$_2$[N_2O_2] (7). Data were collected for a colorless crystal of dimensions 0.28 × 0.50 × 0.80 mm. The compound crystallizes in the monoclinic space group $P2_1/c$ with 2 [quinuclidinium]$_2$[N_2O_2] in the unit cell. A total of 1263 (R_{int} = 0.0351) observed independent reflections [$F > 4\sigma(F)$] were collected in the 2θ range 3.82−49.98°, with the data gathered having $-1 \le h \le 9$, $-1 \le k \le 7$, and $-13 \le l \le 13$. The data were not corrected for absorption. All hydrogen atoms were located in successive Fourier maps and refined isotropically, whereas the non-hydrogen atoms were refined anisotropically. The structure was refined by using the weighted least-squares process $w^{-1} = \sigma^2(F_o^2) + 0.0814^2 + 0.22P$, where $P = (F_o^2 + 4F_c^2)/3$. The maximum and minimum residual intensities remaining were 0.148 and −0.167 e Å^{-3}, respectively.

[2,2′-Bipyridinium][N_2O_2] (8). Data were collected for a colorless crystal of dimensions 0.20 × 0.28 × 0.80 mm. The compound crystallizes in the monoclinic space group $C2/c$ with 4 [2,2′-bipyridinium][N_2O_2] in the unit cell. A total of 905 (R_{int} = 0.0267) observed independent reflections [$F > 4\sigma(F)$] were collected in the 2θ range 4.76−50°, with the data gathered having $-18 \le h \le 1$, $-1 \le k \le 4$,

(16) Sheldrick, G. M. *SHELXTL Crystallographic System*, Version 5.3; Iris Siemens Analytical X-ray Instruments, Inc.: Madison, WI, 1995.

Scheme 1. General Synthetic Scheme for Compounds **1**−**12**

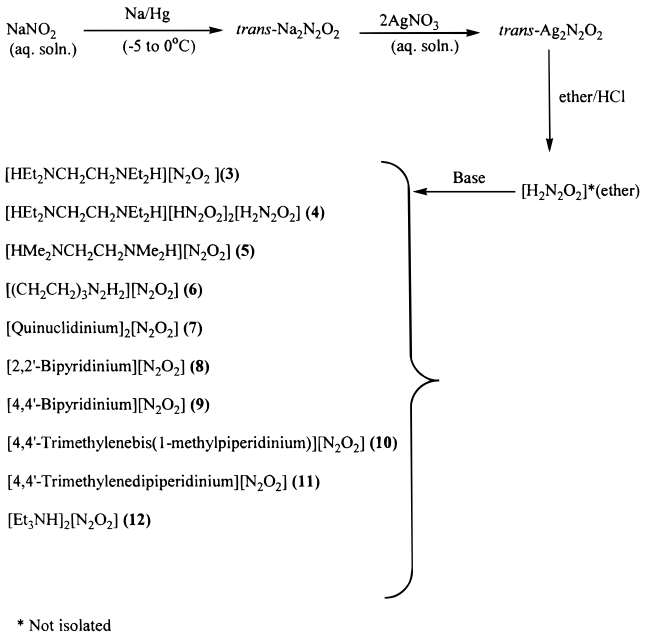

and $-20 \le l \le 22$. The data were not corrected for absorption. All hydrogen atoms were located in successive Fourier maps and refined isotropically, whereas the non-hydrogen atoms were refined anisotropically. The structure was refined by using the weighted least-squares process $w^{-1} = \sigma^2(F_o^2) + 0.0432^2 + 0.46P$, where $P = (F_o^2 + 4F_c^2)/3$. The maximum and minimum residual intensities remaining were 0.149 and -0.154 e Å^{-3}, respectively.

[4,4′-Bipyridinium][N_2O_2] (9). Data were collected for a colorless crystal of dimensions 0.18 × 0.20 × 0.32 mm. The compound crystallizes in the monoclinic space group $P2_1/c$ with 8 [4,4′-bipyridinium][N_2O_2] in the unit cell. A total of 3058 ($R_{int} = 0.0432$) observed independent reflections [$F > 4\sigma(F)$] were collected in the 2θ range 4.42−50°, with the data gathered having $-15 \le h \le 14$, $-1 \le k \le 16$, and $-1 \le l \le 10$. The data were not corrected for absorption. All hydrogen atoms were located in successive Fourier maps and refined isotropically, whereas the non-hydrogen atoms were refined anisotropically. The structure was refined by using the weighted least-squares process $w^{-1} = \sigma^2(F_o^2) + 0.0582^2 + 0.28P$, where $P = (F_o^2 + 4F_c^2)/3$. The maximum and minimum residual intensities remaining were 0.233 and -0.213 e Å^{-3}, respectively.

Results and Discussion

Synthesis. Although the reported yield for compound **1** is usually about 7%, we observe that the yield can be considerably increased to ca. 23% by both cooling the ethanolic solution of sodium hyponitrite in an ice bath for about 2 h and maintaining the solution under an inert atmosphere by passing a stream of nitrogen gas through the headspace as described in the Experimental Section. Unless extraordinary precaution is taken to avoid exposure to CO_2 during the workup and drying of compound **1**, significant contamination and catalytic decomposition by CO_2 were found as has been noted by other workers previously.[9c,17] Compounds **3**−**12** were prepared by mixing anhydrous diethyl ether solution of the appropriate amines and hyponitrous acid except for compounds **9** and **11**, which were prepared by mixing ethanolic solutions of 4,4′-bipyridine and 4,4′-trimethylenedipiperidine, respectively, with hyponitrous acid in diethyl ether. The general synthetic scheme for compounds **1**−**12** is presented in Scheme 1. Dropwise addition of the base to the hyponitrous acid increases the yields. During the synthesis of compound **12**, when less than 1 equiv of triethylamine was added, a monoanionic hyponitrite also containing hyponitrous acid solvated molecules was produced. The mixed hyponitrite compound reacts violently upon exposure to air at room temperature. All these compounds are stable at room temperature for several days, except compound **12,** which is only stable at < -28 °C or at room temperature under inert atmosphere. Excellent analytical data have been obtained for these compounds, except for compounds **4** and **12**, due to their thermal instability under ambient conditions. Compounds **1** and **3**−**12** are soluble in 0.1 M NaOH solution. In addition to their solubility in basic water, compounds **3**−**5**, **7**, and **12** are soluble in a wide range of organic solvents such as tetrahydrofuran, diethyl ether, acetonitrile, acetone, methylene chloride, chloroform, dimethyl sulfoxide, *N*,*N*-dimethylformamide, etc. Furthermore, compound **8** is also soluble in diethyl ether, dichloromethane, acetone, and dimethyl sulfoxide, while compound **9** is soluble in dimethyl sulfoxide. These salts are the first set of hyponitrite salts soluble in organic solvents.

IR, Raman, and UV−Visible Spectral Data. The IR spectra were recorded between 4000 and 400 cm^{-1}. The most notable features in these spectra are the absorption bands around 1000−800 cm^{-1} which are consistent with the presence of the $N_2O_2^{2-}$ anion. By a comparison with the data available for other hyponitrite salts,[18] the following assignments have been made. The spectra exhibit characteristic absorptions at ca. 1000, 800, and 500 cm^{-1}, corresponding to the N−O asymmetric stretch vibrational mode, the out-of-plane NNO symmetric deformation mode, and the N−O out-of-plane bending vibrational mode, respectively. The frequencies of the absorption bands and assignments are presented in Table 3. The N═N stretching vibrational mode is not IR active and is not observed in these spectra. Compounds **3**−**12** also exhibit broad stretching vibrational modes in the 3400−3200 cm^{-1} region, which is indicative of the presence of hydrogen bonding between the hyponitrite oxygen atom and the amine hydrogen atom.

Raman spectra for compounds **3**, **6**, **7**, and **12** were recorded with 632.8 nm laser excitation. A representative spectrum is shown in Figure 2, and hyponitrite vibrational assignments are presented in Table 3. The spectra exhibit medium to strong absorption bands around 1400 cm^{-1} which are assigned to N═N symmetric stretching modes, an intense absorption around 1000−800 cm^{-1} due to N−O symmetric stretching modes, and an intense absorption around 790−600 cm^{-1} assigned to in-plane symmetric deformation. Similar stretching vibrational modes have been reported for other hyponitrite salts.[18]

The UV−visible spectra for compounds **3**−**12** were recorded at room temperature in 0.1 M NaOH solution. All the spectra exhibit a single band at λ_{max} 248 nm, which is characteristic of the hyponitrite anion. This band at 248 nm is most likely an $n \rightarrow \pi^*$ transition. The molar extinction coefficients for these bands correspond to a relatively intense band and span a range from 6800 to 7200 M^{-1} cm^{-1} with an average of 7033 ± 153 M^{-1} cm^{-1}. The molar extinction coefficients for compounds **9** and **10** are not reported, since the bipyridinium chromophore also absorbs in this wavelength region, obscuring the hyponitrite-related $n \rightarrow \pi^*$ transition. The extinction coefficients observed for these compounds are significantly higher than the literature values of 3980,[9a] 6550 ± 200,[9b] and 6550 ± 200 M^{-1} cm^{-1} [9c] reported for sodium hyponitrite in 0.1 M NaOH solution. Since *trans*-sodium hyponitrite obtained from normal preparative

(17) Loechler, E. L.; Schneider, A. M.; Schwartz, D. B.; Hollocher, T. C. *J. Am. Chem. Soc*. **1987**, *109*, 3076.

(18) Okamura, H.; Miki, E.; Mizumachi, K.; Ishimari, T. *Bull. Chem. Soc. Jpn*. **1976**, *49*, 666.

Table 3. Vibrational Spectroscopy Results for Compounds **3**−**12**[a]

compd	ν(OH)	ν(N−N)$_s$(Ram)	ν(N−O)$_{as}$	ν(N−O)$_s$(Ram)	π(ONNO)$_{as}$	δ(NNO)$_s$(Ram)	δ(NO)
3	3437 b	1448 vs	1000 vs	1020 s	741 vs	779.5 s	577 vs
			976 vs			639 vs	463 s
4	3177 b		1010 vs		834 s		465 vs
			988 vs		657 s		
			962 vs				
5	3207 b		1037 vs		831 vs		504 vs
			1020 vs		789 vs		
			989 vs				
6	3434 b	1452 vs	999 vs	985 s	778 vs	623 s	461 vs
7	3443 b	1453 vs	1010 vs	1028 s	777 vs	793 vs	465 vs
			982 vs	1042 s	631 vs		
8	3436 b		1014 vs		765 vs		460 vs
			1004 vs		634 vs		
			989 vs				
9	3453 b		986 vs		809 vs		456 s
					623 vs		
10	3437 b		1001 vs		769 vs		460 vs
11	3453 b		1010 vs		850 vs		459 vs
12	3441 b	1409 vs	1008 vs	1025 s	845 s	737 m	465 vs
			979 vs		804 s		
					670 s		

[a] All bands in cm^{-1}. Raman-active bands denoted (Ram). Abbreviations: vs = strong, s = strong, m = medium, b = broad, subscript "s" = symmetric, subscript "as" = asymmetric.

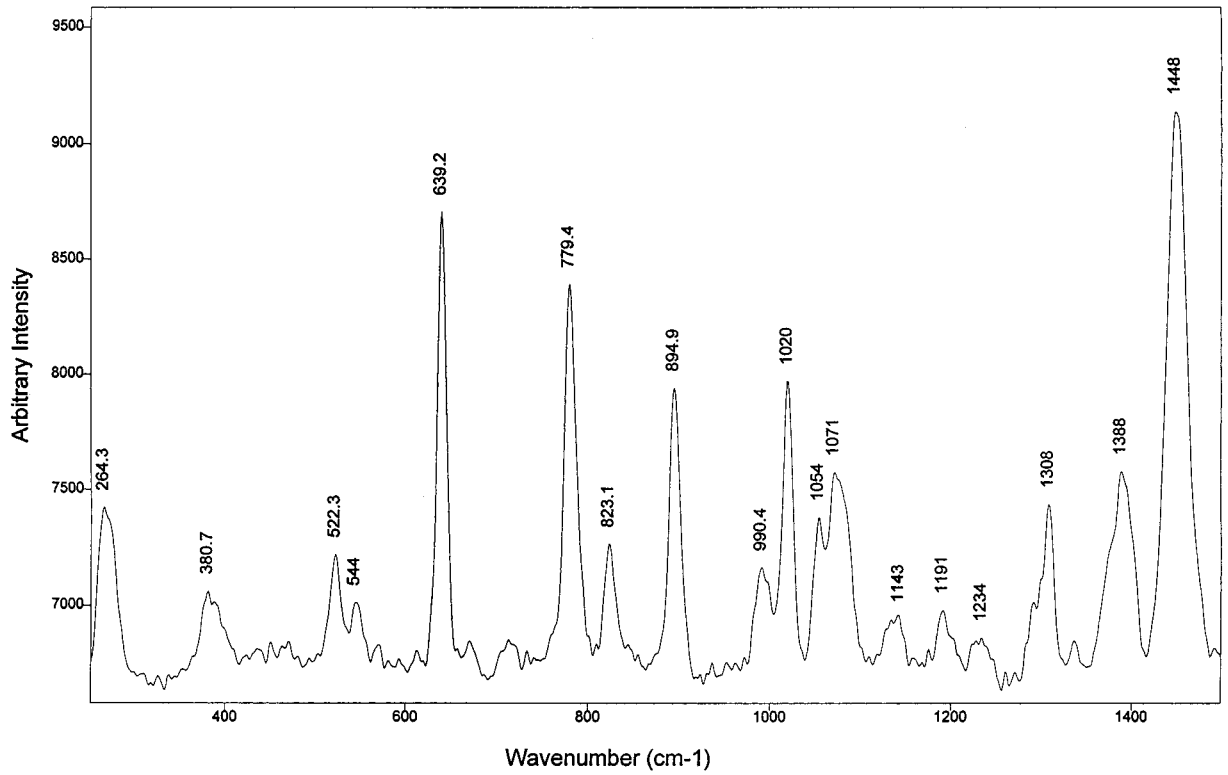

Figure 2. Raman spectrum of $[HEt_2NCH_2CH_2NEt_2H][N_2O_2]$.

methods is usually contaminated with sodium carbonate, the molar extinction coefficient of 6550 ± 200 M^{-1} cm^{-1} should be lower than the actual value owing to the presence of carbonate impurities. The higher molar extinction coefficients observed for these compounds in conjunction with the excellent analytical data indicate that they are carbonate free and therefore should be considered as accurate values of the molar extinction coefficient for the $N_2O_2^{2-}$ anion in 0.1 M NaOH solution.

Structural Data. Compounds **1**, **4**, and **7**−**9** have been characterized by single-crystal X-ray diffraction data −100 °C. Selected bond distances and angles are presented in Table 2.

$Na_2N_2O_2$·5H_2O. The crystal contains sodium ions, coordinated water molecules, and bridging $N_2O_2^{2-}$ anions. The sodium center is hexacoordinate with five water molecules and one hyponitrite ligand. The hyponitrite anion is coordinated to two sodium centers. All the water molecules except one (O(3W)) are coordinated to neighboring sodium atoms as shown in Figure 3. Sodium bridging by water molecules and hyponitrite anions confer a three-dimensional network arrangement. The Na···O distances are in the range 2.3735(8)−2.5638(9) Å. A packing diagram for the structure is shown in Figure 4. In comparison to that of the coordinated water molecules, the interaction between the cation and hyponitrite anion is weaker. A 2-fold axis of symmetry (C_{2v}) passes through the center of the hyponitrite anion. Therefore, a half of the anion is the mirror image of the other and the four atoms of the anion are coplanar. The observed N−N distance of 1.256(2) Å is significantly smaller than a typical N−N double bond. Similarly, the observed

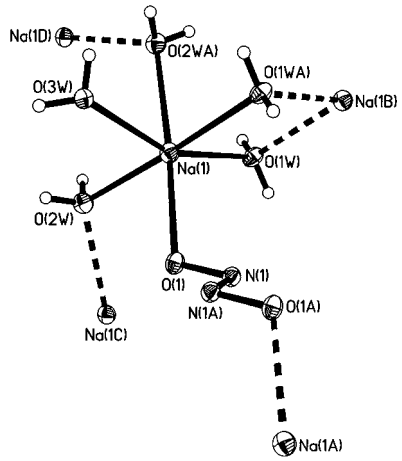

Figure 3. ORTEP view of the sodium coordination environment in $Na_2N_2O_2 \cdot 5H_2O$. All atoms including symmetry equivalents except hydrogen atoms are labeled.

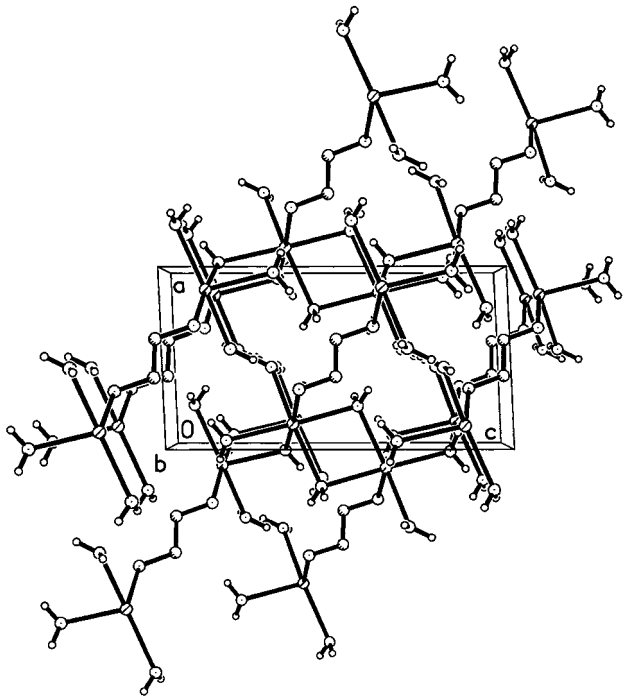

Figure 4. Packing diagram of $Na_2N_2O_2 \cdot 5H_2O$ as viewed along the crystallographic *b* axis.

N−O bond distance of 1.3622(11) Å is also smaller than a typical N−O single bond. These observations together with the planarity of the anion suggest that there is considerable π-bonding delocalized over the whole anion. The di-*tert*-butyl ester of hyponitrous acid also exhibits similar delocalization.[19] The corresponding N═N and N−O distances are 1.252(6) and 1.380(6) Å, respectively, in the ester.[19] The structure of *cis*-sodium hyponitrite as determined from X-ray powder diffraction data is hampered by larger inherent esd's for the N═N and N−O bond distances, 1.20(3) and 1.40(3) Å, respectively.[4] In the latter structure, short Na···N distances, in the range 2.47(3)−3.03(4) Å, are also observed, indicating the involvement of the hyponitrite nitrogen atoms in ionic interactions with the sodium center. The absence of such Na···N interactions together with the delocalization of a double bond in the trans isomer distinguishes the trans from the cis isomer.

$[HEt_2NCH_2CH_2NEt_2H][HN_2O_2]_2 \cdot H_2N_2O_2$. The crystal consists of protonated *N*,*N*,*N*′,*N*′-tetraethylethylenediamine dications

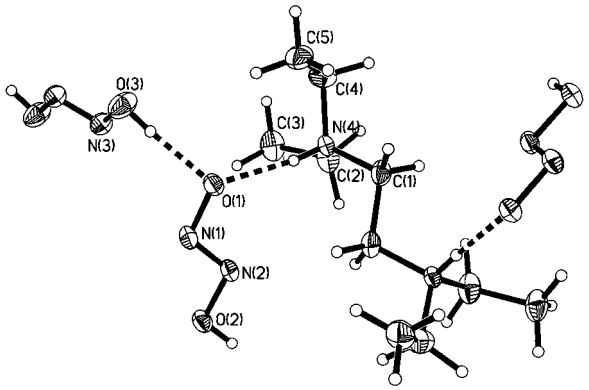

Figure 5. ORTEP view of $[HEt_2NCH_2CH_2NEt_2H][HN_2O_2] \cdot H_2N_2O_2$. All atoms except hydrogen atoms are labeled. The dotted bonds represent hydrogen-bonding interactions.

($[HEt_2NCH_2CH_2NEt_2H]^{2+}$), monoprotonated hyponitrite anions ($[HN_2O_2]^-$) and solvated hyponitrous acid ($H_2N_2O_2$) species. The dication and hyponitrous acid moiety are situated on a 2-fold symmetry axis (C_{2v}), whereas all atoms of the acid molecule are located on general positions. Therefore, the crystallographic asymmetric unit consists of a $[HN_2O_2]^-$ anion and halves of the $[HEt_2NCH_2CH_2NEt_2H]^{2+}$ cation and $H_2N_2O_2$ molecule. Both the monoanion and acid species possess trans geometry.

The observed interatomic distance between the deprotonated oxygen atom of the monoanion (O(1)) and the amine nitrogen atom (N(4)) and that between the former atom and one of the oxygen atoms of the hyponitrous acid molecule at 2.726(3) and 2.592(3) Å, respectively, indicate that the monoanion is involved in hydrogen-bonding interactions with both the cation and acid species as shown in Figure 5. Pairs of neighboring monoanions are also hydrogen-bonded with themselves with the associated O···O distance of 2.648(3) Å. The deprotonated and protonated oxygen atoms of the monoanion serve as hydrogen bond donor and acceptor atoms, respectively. The latter hydrogen-bonding interaction leads to a three-dimensional network arrangement of the species.

The thermal stability observed for this compound at room temperature, despite the presence of hyponitrous acid molecules as solvates in the crystals, could be due to the network arrangement. Hyponitrous acid is known to be extremely unstable at room temperature in the solid state, undergoing violent decomposition.[3a,14] The present compound is the first example of crystallographically characterized hyponitrous acid-containing solid species.

Owing to the excellent quality of the crystallographic data, structural features of the acid and monoanion are well determined, and all hydrogen atoms in the structure have been located in successive Fourier maps and refined isotropically. All atoms, including hydrogen atoms, in the acid molecule are coplanar. Similarly, the monoanion is also planar. As could be expected, the N−O protonated and N−O deprotonated bond distances are considerably different at 1.402(3) and 1.371(3) Å, respectively, in the monoanion. In the acid molecule, the two N−O bond distances are identical at 1.363(3) Å. The observation of a significantly smaller N−O bond distance in the acid molecule in comparison to the analogous distance in the monoanion reveals that the N−N double bond is not localized in the acid molecule. The overall structural features associated with the acid and monoanion species are comparable to those of the hyponitrite ion in the structure of sodium hyponitrite (**1**) and those described below. The $[HEt_2NCH_2CH_2NEt_2H]^{2+}$ dication orients in the trans geometry with respect to the diaminoethane moiety.

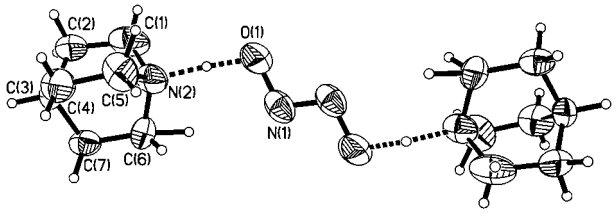

Figure 6. ORTEP view of [quinuclidinium]$_2$[N_2O_2]. All atoms except hydrogen atoms are labeled. The dotted bonds represent hydrogen-bonding interactions.

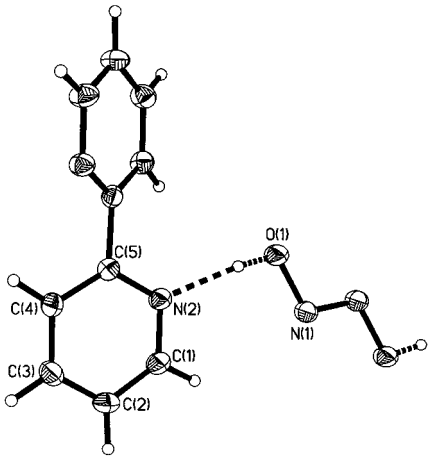

Figure 7. ORTEP view of [2,2′-bipyridinium][N_2O_2]. All atoms except hydrogen atoms are labeled. The dotted bonds represent hydrogen-bonding interactions.

[Quinuclidinium]$_2$[N_2O_2]. The structure consists of well-separated [quinuclidinium]$_2$[N_2O_2] units. As shown in Figure 6, the two *trans*-hyponitrite oxygen atoms are involved in strong hydrogen-bonding interactions with the amine nitrogen atoms of two quinuclidinium cations. A 2-fold symmetry axis (C_{2h}) passes through the center of the hyponitrite anion, and therefore, the four atoms are coplanar. Although the protons are located closer to the hyponitrite oxygen atom (1.260 Å) than the quinuclidine nitrogen atom (1.385 Å), on the basis of the observed relatively short N−O and N−N distances (1.358(3) and 1.224(4) Å, respectively), the species could best be described as a hyponitrite anion and a quinuclidinium cation. The observation of C−N−C angles of 108.7(2), 108.4(2), and 108.3(2)° in the quinuclidinium cation close to the tetrahedral angle is also consistent with this description.

[2,2′-Bipyridinium][N_2O_2]. The structure consists of zigzag chains of hydrogen-bonded [2,2′-bipyridinium][N_2O_2] units as shown in Figure 7. Again the geometry of the hyponitrite ion is trans. Both ions are situated on inversion centers, and therefore, the crystallographic asymmetric unit contains halves of bipyridinium and hyponitrite ions. As in the previous structure, the protons observed between the hyponitrite oxygen and bipyridine nitrogen atom is closer to the oxygen atom (O···H at 0.889 Å) than the nitrogen atom (N···H at 1.804 Å). Still, on the basis of the observed twist of the pyridine rings in the bipyridine moiety, the species could be described as a bipyridinium cation and a hyponitrite anion. Comparison of the structure of 2,2′-bipyridine[20,21] with those of several 2,2′-bipyridinium cations[22−26] reveals that the former possesses a coplanar arrangement of the two pyridine rings, whereas the latter cations prefer a nonplanar geometry for the two pyridine rings. In the present structure, the dihedral angle between the pyridine rings is 36.7°.

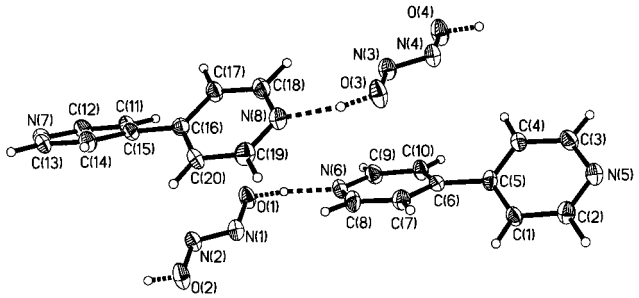

Figure 8. ORTEP view of [4,4′-bipyridinium][N_2O_2]. All atoms except hydrogen atoms are labeled. The dotted bonds represent hydrogen-bonding interactions.

The hyponitrite anion exhibits significant similarity to those in the other structures described in this paper. The observed interatomic distance between the bpy nitrogen atom and hyponitrite oxygen atom at 2.7343(13) Å is indicative of a hydrogen-bonding interaction between the ions. Double hydrogen-bonding interactions between both the cation and anion result in an infinite polymeric chain arrangement of the ions.

[4,4′-Bipyridinium][N_2O_2]. The structure consists of *trans*-hyponitrite anions and 4,4′-bipyridinium cations as shown in Figure 8. The crystallographic asymmetric unit consists of two pairs of the ions, although their overall structural features are comparable. Each of the two pairs of the ions are involved in hydrogen-bonding interactions exclusively within the pairs by means of both their nitrogen and oxygen atoms. The hydrogen-bonding interactions lead to pairs of infinite linear chains. The chains formed by the two crystallographically unique ions are not parallel. The nonparallel orientation of the chains causes the crystallographic dissimilarity between the two pairs of the cations and anions. The pyridine rings in the two bipy cations are not coplanar with observed dihedral angles of 38.9 and 39.2°.

Taken together, the crystallographically observed structural trends for HONNOH, $HONNO^-$, and $^-ONNO^-$ are in good agreement with theoretically calculated geometries from ab initio quantum chemical calculations; see Table 4.[27] For hyponitrous acid, Møller−Plesset level 2 calculations with a 6-31G* basis set predicted a more compact N−N−O bond angle than found for the dianion.[30] However, for this level of theory, both the N−N and N−O calculated bond lengths are longer than observed in the structure of **4**. In part, this could be due to the lack of diffuse functions in this basis set; it is well recognized that the presence of diffuse functions is critical in correctly predicting the ground-state structures of species with mutiple

(19) Jogle, C. A.; VanderKooi, K. A.; Mendenhall, G. D.; Lorprayoon, V.; Cornilson, B. C. *J. Am. Chem. Soc.* **1982**, *104*, 5114.
(20) Merritt, L. L., Jr.; Schroeder, E. D. *Acat Crystallogr.* **1956**, *9*, 801.
(21) Chisholm, M. H.; Huffman, J. C.; Rothwell, I. P.; Bradley, P. G.; Kress, N.; Woodruff, W. H. *J. Am. Chem. Soc.* **1981**, *103*, 4945.
(22) Koda, S.; Ooi, S.; Kuroya, H. *Bull Chem. Soc. Jpn.* **1971**, *44*, 1597.
(23) Nakatsu, K.; Yoshioka, H.; Matsui, M.; Koda, S.; Ooi, S. *Acta Crystallogr.* **1972**, *A28*, S24.
(24) Dorner, H.; Dehnicke, K.; Massa, W.; Schmidt, R. *Z. Naturforsch., B* **1983**, *38*, 437.
(25) Lipkowski, K.; Sgarabotto, P.; Andreetti, G. D. *Cryst. Struct. Commun.* **1976**, *5*, 931.
(26) Stomberg, R.; Szentiranyi, H. *Acta Chem. Scand.* **1984**, *A38*, 121.
(27) Frisch, M. J.; Trucks, G. W.; Schlegel, H. B.; Gill, P. M. W.; Johnson, B. G.; Robb, M. A.; Cheeseman, J. R.; Keith, T.; Petersson, G. A.; Montgomery, J. A.; Raghavachari, K.; Al-Laham, M. A.; Zakrzewski, V. G.; Ortiz, J. V.; Foresman, J. B.; Cioslowski, J.; Stefanov, B. B.; Nanayakkara, A.; Challacombe, M.; Peng, C. Y.; Ayala, P. Y.; Chen, W.; Wong, M. W.; Andres, J. L.; Replogle, E. S.; Gomperts, R.; Martin, R. L.; Fox, D. J.; Binkley, J. S.; Defrees, D. J.; Baker, J.; Stewart, J. P.; Head-Gordon, M.; Gonzalez, C.; Pople, J. A. *Gaussian 94*; Gaussian, Inc.: Pittsburgh, PA, 1995.

Table 4. Contrast in Observed and Calculated Structural Data for *trans*-Hyponitrous Acid and the *trans*-Hyponitrite Dianion

compd	N═N, Å	N−O, Å[a]	N−N−O, deg	method	ref
			trans-Hyponitrous Acid		
4	1.232(3)	1.363(3)	109.9(3)	X-ray crystallography	this report
	1.255	1.399	106.3	MP2/6-31G*	30
	1.2254	1.388	108.23	B3LYP/6-311++G**	this report
			trans-Hyponitrite Dianion		
1	1.256(2)	1.3622(11)	112.14(9)	X-ray crystallography	this report
7	1.224(4)	1.358(3)	110.5(2)	X-ray crystallography	this report
8	1.233(2)	1.3887(13)	107.64(11)	X-ray crystallography	this report
	1.264	1.367	115.4	B3LYP/6-311+G*	this report

[a] Experimental N−O values are for well-ordered species or those for which crystallographic symmetry renders the two bonds equivalent.

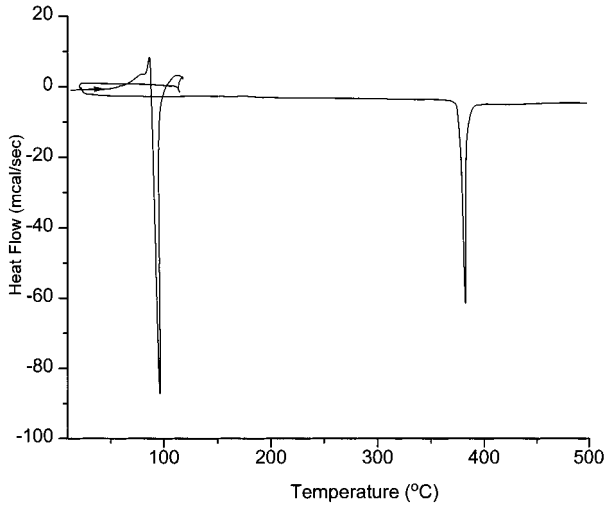

Figure 9. Thermogram of $Na_2N_2O_2 \cdot 5H_2O$, (exothermic transitions down).

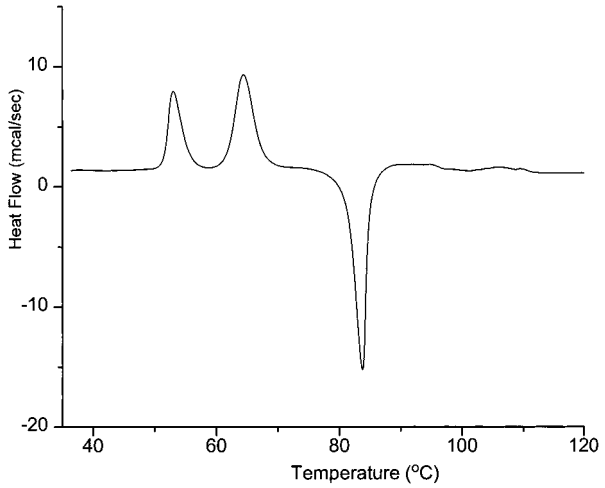

Figure 10. Thermogram of $[HEt_2NCH_2CH_2NEt_2H][N_2O_2]$ (exothermic transitions down).

lone pairs.[28] Significantly, density functional theory with a larger basis set more closely predicts the observed geometry. The effect of including diffuse functions is readily seen in the close match of the B3LYP/6-311+G* results for the trans dianion of hyponitrite[29] and the observed values for **1**, **7**, and **8**. We note however that the ranges found for all of the *trans*-hyponitrite metrical parameters are highly cation dependent.

Differential Scanning Calorimetric Data. The thermal decomposition properties of compounds **1**, and **3**−**12** were studied by differential scanning calorimetry in the temperature region 25−500 °C under a steady stream of argon gas. All these compounds undergo exothermic decomposition in the temperature range 67−382 °C, except compound **6**, which does not decompose exothermically up to 500 °C and instead exhibits a small endotherm at 196 °C. Representative DSC traces are presented in Figures 9 and 10, and the data are presented in Table 5.

The thermogram of crystalline samples of sodium hyponitrite, **1**, dried in a desiccator, exhibits two exotherms at 96 and 382 °C. This is the first time that this thermal behavior has been reported. In contrast, Abata et al.[10c] have reported that the same anhydrous salt undergoes exothermic decomposition at a single temperature, namely 382 °C, while also exhibiting a small endothermic transition at ca. 100 °C.[10c] Our subsequent experiments on samples of **1**, dried over P_2O_5 at ca. 50 °C under reduced pressure, reveal that these samples reproduce the results of Abata et al.[10c] The samples dried under reduced pressure lost their crystalline nature and were powdery.

Table 5. Differential Scanning Calorimetric Data for **1** and **3**−**12**

compd	T_{onset}, °C	T_{max}, °C	dec range, °C	ΔH, cal/g	ΔH, kcal/mol
1	86.50	95.10	86.50−106.37	−170.1	−28.87
	377.47	382.45	377.45−399.84	−102.3	
3[a]	81.20	83.69	81.09−84.97	−28.32	−6.64
4	81.12	83.38	81.12−88.16	−93.73	−33.59
5[b]	106.38	107.88	106.38−112.12	−1.52	−0.27
6[c]					
7	88.50	94.31	88.50−95.60	−46.75	−13.24
8	149.64	152.03	149.64−154.31	−28.98	−6.32
9	166.68	170.81	166.68−174.50	−52.37	−11.43
10	128.28	130.85	128.28−142.00	−16.29	−4.89
11	121.91	123.90	121.92−131.00	−13.78	−3.75
12	62.41	67.37	62.41−76.50	−73.68	−19.45

[a] Two endothermic processes were also observed at 53.08 and 64.51 °C. [b] An endothermic process was also observed at 106.38 °C. [c] This compound was thermally stable and exhibited a mild endothermic process at 191.53 °C.

To explain the significantly different DSC behavior of the crystalline sodium hyponitrite samples, the following experiments were carried out. (1) A thermogram was obtained in the temperature range −100 +25 °C; the thermogram did not exhibit any peaks. (2) To determine the nature of the exotherm at 96 °C, a thermal cycle was performed between 25 and 110 °C, followed by heating to 500 °C. The thermogram obtained is shown in Figure 9. The thermogram demonstrates the irreversibility of the thermal process associated with the first exotherm, ruling out the occurrence of reversible solid-state phase transition. However, the exotherm can only be explained on the basis

(28) Clark, T.; Chandrasekhar, J.; Spitznagel, G. W.; Schleyer, P. v. R. *J. Comput. Chem.* **1983**, *4*, 294−301.
(29) Sins, A.; Panas, I. *Chem. Phys.* **1997**, *221*, 1−10.
(30) Brown, R. E.; Mendenhall, G. D.; Bartlett, R. J. *Int. J. Quantum Chem. Quantum Chem. Symp.* **1987**, *21*, 603−612.

of coupled irreversible solid-state phase transition and dehydration. The observation of a small endothermic peak close to the first exotherm in the forward scan is consistent with the above conclusion. Powder X-ray diffraction of the sample (not shown) demonstrates that the original lattice is completely shattered upon dehydration but that the resulting phase is still crystalline, but in a new and undetermined lattice. A close inspection of the packing diagram of **1** (Figure 4) reveals that the water molecules in the crystal are solely responsible for the three-dimensional network arrangement, and therefore it is reasonable to expect a drastic phase transition resulting from dehydration of the crystals. (3) Another experiment was performed by rehydrating the powdered compound **1** in a CO_2-free atmosphere and scanning from 25 to 500 °C. A broad endotherm at 100 °C corresponding to the loss of water of hydration and an exotherm at 382 °C were observed. These observations suggest that it is the crystalline phase transition that is responsible for the exotherm at ca. 100 °C.

The second exothermic decomposition observed at ca. 382 °C is identical to the decomposition of anhydrous sodium hyponitrite reported by Abata et al.[10c] As previously observed by Abata et al.[10c] a white residue was left in the cup after decomposition.

The thermogram of **3** exhibits two endotherms at 53.05 and 64.51 °C and an exotherm at 83.69 °C as shown in Figure 10. A thermal cycle was also performed between 25 and 68 °C, followed by heating again to 500 °C. The absence of the two endotherms in the second forward scan indicates that these processes are irreversible. Compound **5** also exhibits an endothermic process at 106.38 °C that merges with an exothermic process at 107.88 °C. From Table 5, the thermal stability of **3**−**5** and **7**−**12** increases progressively as the size of the cation increases. The effect of the size of the cation on the thermal stability of the salt may be ascribed to the increase in the hydrogen interactions between the cations and the hyponitrite anions. The thermal decomposition reactions of compounds **3**−**12** left no solid residue in the cup. Similar observations have been reported for ammonium and guanidinium hyponitrites.[10b]

Electrochemistry. As a consequence of the general insolubility of $[N_2O_2]^{2-}$ salts in organic solvents, their nonaqueous electrochemistry has never been reported. With the synthesis of these hyponitrites having distinctive solubility in a wide variety of organic solvents, we investigated the redox properties of the $[N_2O_2]^{2-}$ anion for the first time. The redox behavior of the $[N_2O_2]^{2-}$ anion was studied by cyclic and square-wave voltammetric techniques using a platinum-button working electrode in acetonitrile containing 0.1 M TBAP as the supporting electrolyte and an Ag/AgCl reference electrode. A few drops of triethylamine or pyridine were equally added to keep the solution slightly basic. The $[N_2O_2]^{2-}$ anion exhibited an irreversible oxidation process at 1.78 V at a scan rate of 100 mV/s or at 2.1 V at a scan rate of 200 mV/s. Similar irreversible redox behavior has been observed for the peroxynitrite $[ONOO]^-$ anion in acetonitrile.[31]

Conclusions

The structural data obtained for sodium hyponitrite confirm the trans geometry for the hyponitrite anion predicted on the basis of IR and Raman spectral data.[3,5] The DSC of crystalline *trans*-$Na_2N_2O_2 \cdot 5H_2O$ exhibits two exothermic processes at ca. 96 and 382 °C. Anhydrous powdery $Na_2N_2O_2$ exhibits a single exothermic process at 382 °C, in good agreement with the results of Abata et al.[10c] These results unambiguously clarify the discrepancies surrounding the thermal behavior of *trans*-sodium hyponitrite.[3a,9a,10]

We have synthesized novel alkylammonium hyponitrites and base-stabilized monoprotonated hyponitrite and hyponitrous acid salts. Compounds **3**−**5**, **7**, and **12** exhibit distinctive solubilities in a wide variety of aprotic solvents which allow us to electrochemically investigate the redox behavior of the hyponitrite dianion under nonaqueous conditions for the first time. The average molar extinction coefficients of $7033 \pm 153\ M^{-1}\ cm^{-1}$ in 0.1 M NaOH is an accurate molar extinction coefficient for the hyponitrite dianion. The single-crystal X-ray crystallographic results for compounds **1**, **4**, and **7**−**9** also support the result from vibrational spectroscopic evidence that the most stable geometry of hyponitrite is the trans geometry.[3,5] In addition to the planarity of the four atoms in the hyponitrite anion, there is considerable π-bonding over the four-atom framework. Compounds **3**−**5** and **7**−**12** exhibit a single exothermic process from 67 to 170 °C. A progressive increase in the thermal stability was observed for compounds **3**−**5** and **7**−**12** as the size of the cation increased. The thermal stability conferred on these hyponitrites as the size of the cation increased may be due to an increase in the hydrogen-bonding interactions between the cation and the hyponitrite anion. These compounds exhibit an irreversible redox behavior.

Acknowledgment. We gratefully acknowledge support from the NIH (Grant GM-53828), the NSF (Grant CHE-9807860), and the Air Force Office of Scientific Research (Grants F49620-96-1-0417 and -98-1-0461).

Supporting Information Available: Tables listing detailed crystallographic data, atomic positional parameters, bond lengths and angles, and anisotropic displacement parameters. This material is available free of charge via the Internet at http://pubs.acs.org.

IC981340C

(31) Sand, P. Masters Thesis, University of Wyoming, Laramie, WY, 1997.